J|A|C|S
ARTICLES
Published on Web 04/18/2002

Pressure-Induced Volume Expansion of Zeolites in the Natrolite Family

Yongjae Lee,[†] Thomas Vogt,*[,†] Joseph A. Hriljac,[‡] John B. Parise,[§] and Gilberto Artioli[⊥]

Contribution from the Physics Department, Brookhaven National Laboratory, Upton, New York 11973-5000, School of Chemical Sciences, University of Birmingham, Birmingham, B15 2TT, UK, Geosciences Department, State University of New York, Stony Brook, New York 11794-2100, and Dipartimento di Scienze della Terra, Università degli Studi di Milano, Via Botticelli 23, I-20133 Milano, Italy

Received January 15, 2002

Abstract: Powder diffraction patterns of the zeolites natrolite ($Na_{16}Al_{16}Si_{24}O_{80}\cdot 16H_2O$), mesolite ($Na_{5.33}Ca_{5.33}Al_{16}Si_{24}O_{80}\cdot 21.33H_2O$), scolecite ($Ca_8Al_{16}Si_{24}O_{80}\cdot 24H_2O$), and a gallosilicate analogue of natrolite ($K_{16}Ga_{16}Si_{24}O_{80}\cdot 12H_2O$), all crystallizing with a natrolite framework topology, were measured as a function of pressure up to 5.0 GPa with use of a diamond-anvil cell and a 200 μm focused monochromatic synchrotron X-ray beam. Under the hydrostatic conditions mediated by an alcohol and water mixture, all these materials showed an abrupt volume expansion (ca. 2.5% in natrolite) between 0.8 and 1.5 GPa without altering the framework topology. Rietveld refinements using the data collected on natrolite show that the anomalous swelling is due to the *selective sorption* of water from the pressure-transmission fluid expanding the channels along the *a*- and *b*-unit cell axes. This gives rise to a "superhydrated" phase of natrolite with an approximate formula of $Na_{16}Al_{16}Si_{24}O_{80}\cdot 32H_2O$, which contains hydrogen-bonded helical water nanotubes along the channels. In mesolite, which at ambient pressure is composed of ordered layers of sodium- and calcium-containing channels in a 1:2 ratio along the *b*-axis, this anomalous swelling is accompanied by a loss of the superlattice reflections ($b_{mesolite} = 3b_{natrolite}$). This suggests a pressure-induced order−disorder transition involving the motions of sodium and calcium cations either through cross-channel diffusion or within the respective channels. The powder diffraction data of scolecite, a monoclinic analogue of natrolite where all sodium cations are substituted by calcium and water molecules, reveal a reversible pressure-induced partial amorphization under hydrostatic conditions. Unlike the 2-dimensional swelling observed in natrolite and mesolite, the volume expansion of the potassium gallosilicate natrolite is 3-dimensional and includes the lengthening of the channel axis. In addition, the expanded phase, stable at high pressure, is retained at ambient conditions after pressure is released. The unprecedented and intriguing high-pressure crystal chemistry of zeolites with the natrolite framework topology is discussed here relating the different types of volume expansion to superhydration.

Introduction

Zeolites are naturally occurring aluminosilicate materials crystallizing in a variety of low-density framework structures constructed from corner-connected (Al,SiO_4)-tetrahedra. These units define windows with a narrow size-distribution of pores and channels of molecular dimensions.[1] It is the restricted access to the interior that provides the reactant, transition state, and product selectivity. This selectivity makes these "nanoreactors" valuable selective heterogeneous catalysts and ion exchangers in a number of industrial and environmental applications. The built-in flexibility of the T−O−T angle connector between tetrahedral units allows these structures to contract and expand in response to thermodynamic variables such as temperature and pressure.

While an ever-expanding variety of zeolites with a wide range of pore sizes is available, it is desirable to have a way to vary the chemistry of the zeolitic nanopores for a given framework topology and provide selective access to the interior for ion exchange and sorption. Temperature has been used almost exclusively to control the degree of hydration and hydroxylation, remove templating molecules after synthesis, facilitate ion exchange or gas separation processes, or to control the cation distributions within the pores.[2−5] However, modifications of the nanopores using temperature may compromise the mechanical

* Corresponding author. E-mail: yollee@bnl.gov; tvogt@bnl.gov.
[†] Brookhaven National Laboratory.
[‡] University of Birmingham.
[§] State University of New York.
[⊥] Università degli Studi di Milano.

(1) Breck, D. W. *Zeolite Molecular Sieves*; Krieger: Malabar, FL, 1984.
(2) Barrer, R. M. *Hydrothermal Chemistry of Zeolites*; Academic Press: London, 1982.
(3) Baur, W. H.; Joswig, W. *N. Jb. Miner. Mh.* **1996**, 171−187.
(4) Miyamoto, T.; Katada, N.; Kim, J. H.; Niwa, M. *J. Phys. Chem.* **1998**, *102*, 6738−6745.
(5) Lee, Y.; Reisner, B. A.; Hanson, J. C.; Jones, G. A.; Parise, J. B.; Corbin, D. R.; Toby, B. H.; Freitag, A.; Larese, J. Z.; Kahlenberg, V. *J. Phys. Chem.* **2001**, *B105*, 7188−7199.

10.1021/ja0255960 CCC: $22.00

integrity of the whole atomic scaffolding, and indeed, in many cases the metastable frameworks collapse to dense structures below the corresponding glass transition temperatures, the upper limit for the temperature-driven applications. For those classes of zeolites with relatively dense framework structures, such as natrolite and related analogues,[6] the limited access to the internal pores makes facile and reversible tuning of the nanopore chemistry, using temperature alone, difficult.

The crystal chemistry of zeolites under moderately high pressures, say below 5 GPa, is not similar to that observed in temperature-dependent studies. For example, inverse-pressure effects such as anomalous volume expansion and an increase in water diffusivity have been reported in natrolite and its analogues,[7,8] the mechanism of which remained unknown prior to our recent preliminary communication.[9] Our investigations focus on the structures of zeolites at hydrostatic pressures. Pressure can be used to alter both the crystal structures without leading to a collapse of the framework as well as the nanopore chemistry of zeolites via interactions with the hydrostatic pressure transmission fluid.[9,10] We have found that the compressibility and phase transition kinetics of zeolite rho are dependent upon the charge compensating cations and their distributions within the pores.[10] We have discovered that the volume expansion of natrolite at high pressure occurs through selective sorption of water molecules from the hydrostatic pressure fluid, giving rise to a superhyrated phase with twice the water content.[9] This anomalous volume expansion at high pressure is particularly intriguing since it results in the formation of a new water structure inside the walls of the nanochannels and is responsible for the increased water diffusion at high pressures.[8] In addition, the expanded pore openings through the channel swelling under pressure may dramatically alter the ion exchange and other sorption properties of this small-pore zeolite. Following the original high-pressure study performed on natrolite, we have extended our work to closely related framework materials mesolite and scolecite to investigate the influences nonframework cations have on the structural chemistry of these materials. Studies of a potassium gallosilicate analogue of natrolite allow the investigation of changes in the framework composition on pressure-induced volume expansion.

Natrolite, as well as mesolite and scolecite, belongs to the group of fibrous, small-pore zeolites with a natrolite topology.[6] This framework is composed of T_5O_{10} building units formed from linking five TO_4 tetrahedra (T = Al, Si, Ga, ...). These units are then connected along the *c*-axis to form the so-called natrolite chains (Figure 1). The mode of linkage of the chains to each other is conveniently described by the heights in eighths of a unit cell translation above the *xy*-plane of the central tetrahedral nodes of the T_5O_{10} building units (*h* in Figure 1). Natrolite shows a *2460*-type linkage in the four neighboring chains (Figure 1).[11] As a result, helical 8-ring channels are formed along the *c*-axis with $T_{10}O_{20}$ windows intersecting

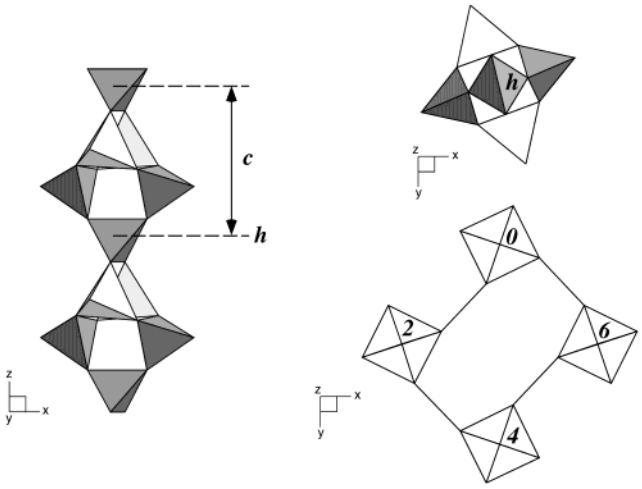

Figure 1. A polyhedral representation of the chain found in the natrolite framework (left). The repeat distance of the T_5O_{10} building unit of the Si− (shaded) and Al− (unshaded) tetrahedra constitutes the *c*-axis length (*c*). The height (*h*) of the 4-connected tetrahedral node (upper right) can be described in terms of eighths of the repeat distance and natrolite shows a *2460*-type connectivity of the neighboring chains (skeletal representation in lower right, see text).

perpendicular to these channels. The flexible linkages between and within the chains and their interactions with charge-balancing cations and water molecules give rise to various structural distortions depending on composition and temperature.[3,12,13] A distortion parameter, ψ, which measures the average angle between the T_5O_{10} building unit and the *a*- and *b*-unit-cell axes, can specify the degree of chain rotation.[12] Under ambient conditions, the aluminosilicate natrolite (ideal chemical composition: $Na_{16}Al_{16}Si_{24}O_{80}\cdot 16H_2O$) has an ordered distribution of Al and Si over the T-sites in *Fdd*2 (orthorhombic) symmetry with sodium cations along the channels and water molecules close to the $T_{10}O_{20}$ windows. Scolecite ($Ca_8Al_{16}Si_{24}O_{80}\cdot 24H_2O$) is a natural Ca-endmember of natrolite where the substitution of all Na cations by Ca and water causes a lowering of the unit cell symmetry from orthorhombic *Fdd*2 to pseudoorthorhombic *Fd* (monoclinic).[14] Mesolite ($Na_{5.33}Ca_{5.33}Al_{16}Si_{24}O_{80}\cdot 21.33H_2O$) is a natural analogue of natrolite where $^2/_3$ of the Na cations in natrolite are replaced by Ca and H_2O.[15] The structure of mesolite is composed of one natrolite-like and two scolecite-like layers alternating along the *b*-axis, resulting in a superlattice structure ($b_{\text{mesolite}} = 3b_{\text{natrolite}}$) with *Fdd*2 symmetry and a tripling of the unit cell composition to $Na_{16}Ca_{16}Al_{48}Si_{72}O_{240}\cdot 64H_2O$. The potassium gallosilicate ($K_{16}Ga_{16}Si_{24}O_{80}\cdot 12H_2O$) is a synthetic natrolite where Na and Al are substituted by K and Ga, respectively.[13] The resulting crystal structure differs from that of natrolite by a disordered distribution of Ga and Si over the framework tetrahedral sites to give rise to a $I\bar{4}2d$ (tetragonal) symmetry and a unit cell composition of $K_8Ga_8Si_{12}O_{40}\cdot 6H_2O$. In contrast to the Na and H_2O distribution in natrolite, potassium cations occupy the sites bound by the $T_{10}O_{20}$ windows close to the channel walls and water molecules are found along the channels.[13]

(6) Baerlocher, C.; Meier, W. M.; Olson, D. H. *Atlas of Zeolite Framework Types*, 4th ed.; Elsevier: Amsterdam, The Netherlands, 2001.
(7) Belitsky, I. A.; Fursenko, B. A.; Gubada, S. P.; Kholdeev, O. V.; Seryotkin, Y. V. *Phys. Chem. Miner.* **1992**, *18*, 497−505.
(8) Moroz, N. K.; Kholopov, E. V.; Belitsky, I. A.; Fursenko, B. A. *Microporous Mesoporous Mater.* **2001**, *42*, 113−119.
(9) Lee, Y.; Hriljac, J. A.; Vogt, T.; Parise, J. B.; Artioli, G. *J. Am. Chem. Soc.* **2001**, *123*, 12732- 12733.
(10) Lee, Y.; Hriljac, J. A.; Vogt, T.; Parise, J. B.; Edmondson, M. J.; Anderson, P. A.; Corbin, D. R.; Nagai, T. *J. Am. Chem. Soc.* **2001**, *123*, 8418−8419.
(11) Smith, J. V. *Z. Kristallogr.* **1983**, *165*, 191−198.
(12) Baur, W. H.; Kassner, D.; Kim, C.-H.; Sieber, N. H. *Eur. J. Mineral.* **1990**, *2*, 761−769.
(13) Lee, Y.; Kim, S. J.; Parise, J. B. *Microporous Mesoporous Mater.* **2000**, *34*, 255−271.
(14) Kvick, A.; Stahl, K.; Smith, J. V. *Z. Kristallogr.* **1985**, *171*, 141−154.
(15) Artioli, G.; Smith, J. V.; Pluth, J. J. *Acta Crystallogr.* **1986**, *C42*, 937−942.

Table 1. Final Refined Atomic Coordinates for Natrolite as a Function of Pressure[a]

		0.40 GPa	0.84 GPa	1.51 GPa	1.72 GPa	2.42 GPa	3.58 GPa	5.01 GPa
space group		*Fdd2*	*Fdd2*	*Fdd2*	*Fdd2*	*Fdd2*	*Fdd2*	*Fdd2*
DLS *R*-value[b]		0.0029	0.0029	0.0028	0.0028	0.0031	0.0035	0.0040
$_wR_p$ (%), R_p (%), χ^2		4.5, 2.9, 1.3	5.6, 3.9, 1.0	5.2, 3.4, 1.2	4.1, 2.6, 1.1	6.7, 3.4, 3.6	4.6, 3.0, 1.5	4.5, 2.9, 1.4
cell length (Å)	*a*	18.226(2)	18.180(4)	18.390(6)	18.378(3)	18.233(3)	18.097(2)	17.924(2)
	b	18.583(2)	18.531(4)	18.829(6)	18.818(3)	18.679(3)	18.518(2)	18.325(2)
	c	6.579(1)	6.566(2)	6.547(2)	6.545(1)	6.530(1)	6.512(1)	6.487(1)
Si(1): *8a*	*x*	0	0	0	0	0	0	0
Si(2): *16b*	*x*	0.1493(1)	0.1491(1)	0.1536(1)	0.1534(1)	0.1505(4)	0.1510(2)	0.1507(2)
	y	0.2168(1)	0.2177(1)	0.2106(1)	0.2107(1)	0.2134(4)	0.2128(2)	0.2128(2)
	z	0.6180(2)	0.6177(2)	0.6172(2)	0.6172(1)	0.6173(9)	0.6175(3)	0.6166(3)
Al: *16b*	*x*	0.0338(1)	0.0331(1)	0.0400(1)	0.0399(1)	0.0376(4)	0.0375(2)	0.0368(2)
	y	0.0975(1)	0.0977(1)	0.0929(1)	0.0930(1)	0.0952(4)	0.0957(2)	0.0963(2)
	z	0.6095(2)	0.6097(2)	0.6099(2)	0.6099(1)	0.6085(9)	0.6098(3)	0.6103(3)
O(1): *16*b	*x*	0.0170(4)	0.0131(3)	0.0400(3)	0.0400(2)	0.0383(8)	0.0404(4)	0.0435(3)
	y	0.0695(1)	0.0705(1)	0.0588(2)	0.0588(1)	0.0605(5)	0.0602(3)	0.0590(2)
	z	0.8592(2)	0.8589(2)	0.8586(2)	0.8585(1)	0.8577(9)	0.8587(4)	0.8579(3)
O(2): *16b*	*x*	0.0662(1)	0.0660(1)	0.0711(1)	0.0708(1)	0.0668(4)	0.0659(2)	0.0641(2)
	y	0.1861(1)	0.1864(1)	0.1807(1)	0.1809(1)	0.1844(4)	0.1860(2)	0.1879(2)
	z	0.6080(3)	0.6078(3)	0.6079(3)	0.6079(2)	0.6090(16)	0.6077(6)	0.6072(6)
O(3): *16b*	*x*	0.0991(1)	0.0995(1)	0.0968(1)	0.0969(1)	0.0969(6)	0.0963(3)	0.0946(3)
	y	0.0404(2)	0.0398(2)	0.0408(1)	0.0410(1)	0.0444(4)	0.0450(2)	0.0467(2)
	z	0.4997(9)	0.5072(7)	0.4565(6)	0.4564(3)	0.4556(19)	0.4525(8)	0.4439(7)
O(4): *16b*	*x*	0.2018(2)	0.2025(2)	0.2011(1)	0.2009(1)	0.1980(4)	0.1967(2)	0.1942(2)
	y	0.1569(1)	0.1568(1)	0.1596(1)	0.1596(1)	0.1606(6)	0.1597(3)	0.1600(3)
	z	0.7219(9)	0.7143(7)	0.7650(6)	0.7652(3)	0.7634(18)	0.7686(8)	0.7772(7)
O(5): *16b*	*x*	0.1791(1)	0.1781(1)	0.1898(2)	0.1897(1)	0.1878(5)	0.1885(3)	0.1900(2)
	y	0.2335(4)	0.2374(3)	0.2111(3)	0.2111(2)	0.2126(7)	0.2105(4)	0.2072(3)
	z	0.3909(2)	0.3912(2)	0.3917(2)	0.3917(1)	0.3915(9)	0.3917(4)	0.3922(3)
Na: *16b*	*x*	0.220(1)	0.221(1)	0.224(1)	0.224(1)	0.217(1)	0.228(2)	0.225(1)
	y	0.035(1)	0.036(1)	0.028(1)	0.029(1)	0.029(1)	0.024(1)	0.025(1)
	z	0.623(2)	0.638(4)	0.629(5)	0.599(4)	0.557(4)	0.615(3)	0.623(3)
OW1: *16b*	*x*	0.059(1)	0.054(2)	0.055(2)	0.055(2)	0.065(2)	0.061(1)	0.060(1)
	y	0.190(1)	0.184(2)	0.181(2)	0.180(1)	0.178(2)	0.182(1)	0.186(1)
	z	0.110(4)	0.139(8)	0.12(1)	0.107(8)	0.113(9)	0.113(7)	0.117(6)
OW2: *16b*	*x*			0.184(2)	0.180(2)	0.190(1)	0.180(1)	0.181(1)
	y			0.071(2)	0.066(1)	0.067(2)	0.070(1)	0.081(1)
	z			0.110(6)	0.086(5)	0.054(6)	0.110(4)	0.088(4)

[a] Esd's are in parentheses. Fixed isotropic displacement parameters, U_{iso} (Å^2), were used for all models (0.017 and 0.022 for framework and extraframework elements, respectively). All sites are fully occupied. [b] Generated from starting framework models.

As mentioned earlier, natrolite and the related analogues are examples of small-pore zeolites into which both cation and water access are hindered. Most of the studies on their cation exchange properties came to the conclusion that a very limited exchange occurs in aqueous solutions below 100 °C and that the highest exchange levels have been observed in fused salt studies.[16] Large radioisotopes such as ^{90}Sr and ^{137}Cs simply cannot access the narrow pores of natrolite at ambient conditions. It is also well-known that natrolite does not take up any significant amounts of smaller transition metal cations such as Co, Ni, Cd, and Zn. Although mesolite and scolecite are calcium-containing members of the natrolite group, substitution of sodium with calcium is not possible under normal ion exchange conditions.[16] The reason may lie in the unusual 7-fold coordination environment for calcium and other divalent cations in the natrolite framework as opposed to the preferred 6-fold coordination of sodium, which will make the substitution of two sodium cations by a divalent cation and a water molecule energetically unfavorable. It is also suggested that the interchannel diffusion via the $T_{10}O_{20}$ windows of the channel walls may be the limiting factor for ion exchange applications in the natrolite group materials. Superhydration and associated channel expansion observed in natrolite at high pressure opens up a new path to modify both the nanopore geometry and chemistry within and may provide novel and unprecedented applications for these small-pore zeolites. We report here the novel crystal chemistry of the natrolite-based materials at high pressure using a diamond-anvil cell (DAC) and a 200 μm focused monochromatic synchrotron X-ray beam.

Experimental Section

Experiments were performed using a Diamond Anvil Cell (DAC) at the X7A beamline of the National Synchrotron Light Source (NSLS) at Brookhaven National Laboratory (BNL). The primary white beam from the bending magnet is focused in the horizontal plane by a triangular, asymmetrically cut Si (220) monochromator bent to cylindrical curvature by applying a load to the crystal tip, affording microfocused (~200 μm) monochromatic radiation of ~0.7 Å.[17] A tungsten wire crosshair was positioned at the center of the goniometer circle and subsequently the position of the incident beam was adjusted to the crosshair. A gas-proportional position-sensitive detector[18] was stepped in 0.25° intervals over the angular range of 3−35° with counting times of 90−150 s per step. The wavelength of the incident beam (0.7054-(1) Å for the natrolite run and 0.6942(1) Å for all other measurements), PSD zero channel, and PSD degrees/channel were determined from a CeO_2 standard (SRM 674).

Powdered samples of the mineral natrolite (from Dutoitspan, South Africa, EPMA: $Na_{16}Al_{16}Si_{24}O_{80}\cdot 16H_2O$), mesolite (Poona, India, EPMA: $Na_{4.8}Ca_{5.1}Al_{15.4}Si_{24.0}O_{80}\cdot 21.3H_2O$), scolecite (Nasik, India, EPMA: $Ca_{8.1}Al_{15.7}Si_{24.0}O_{80}\cdot 24H_2O$), and a synthetic gallosilicate ana-

(16) Dyer, A.; Faghihian, H. *Microporous Mesoporous Mater.* **1998**, *21*, 27−38.

(17) Lemonnier, M.; Fourme, R.; Rosseaux, F.; Kahn, R. *Nucl. Instrm. Methods* **1978**, *152*, 173- 177.

(18) Smith, G. C. *Synch. Rad. News* **1991**, *4*, 24−30.

Table 2. Selected Interatomic Distances (Å) and Angles (deg) for Natrolite as a Function of Pressure[a]

	0.40 GPa	0.84 GPa	1.51 GPa	1.72 GPa	2.42 GPa	3.58 GPa	5.01 GPa
Si(1)−O(1)	1.6198(3)	1.6199(2)	1.6200(3)	1.6200(1)	1.6211(13)	1.6199(5)	1.6201(5)
Si(1)−O(5)	1.6198(3)	1.6199(2)	1.6200(3)	1.6200(1)	1.6213(13)	1.6199(5)	1.6200(5)
mean	1.6198(2)	1.6199(1)	1.6200(2)	1.6200(2)	1.6212(9)	1.6199(4)	1.6201(4)
Si(2)−O(2)	1.6197(4)	1.6197(3)	1.6198(4)	1.6197(2)	1.6199(18)	1.6196(7)	1.6196(7)
Si(2)−O(3)	1.6198(4)	1.6198(3)	1.6198(4)	1.6198(2)	1.6205(18)	1.6197(7)	1.6201(7)
Si(2)−O(4)	1.6197(4)	1.6198(3)	1.6198(4)	1.6198(2)	1.6213(18)	1.6197(7)	1.6197(7)
Si(2)−O(5)	1.6198(4)	1.6198(4)	1.6198(4)	1.6198(2)	1.6235(18)	1.6199(7)	1.6198(7)
mean	1.6198(2)	1.6198(2)	1.6198(2)	1.6198(1)	1.6213(9)	1.6197(4)	1.6198(4)
Al−O(1)	1.7498(4)	1.7498(4)	1.7498(4)	1.7498(2)	1.7521(18)	1.7499(7)	1.7500(7)
Al−O(2)	1.7497(4)	1.7497(3)	1.7498(4)	1.7497(2)	1.7493(18)	1.7493(7)	1.7494(7)
Al−O(3)	1.7498(4)	1.7498(3)	1.7498(4)	1.7498(2)	1.7519(18)	1.7498(7)	1.7500(7)
Al−O(4)	1.7497(4)	1.7498(3)	1.7498(4)	1.7498(2)	1.7503(18)	1.7497(7)	1.7498(7)
mean	1.7498(2)	1.7498(2)	1.7498(2)	1.7498(1)	1.7509(9)	1.7497(4)	1.7498(4)
Si(1)−O(1)−Al	143.8(1)	142.9(1)	141.5(1)	141.4(1)	141.9(5)	140.4(2)	138.6(2)
Si(2)−O(2)−Al	130.3(2)	130.9(2)	129.3(1)	129.2(1)	127.2(4)	125.0(2)	122.5(1)
Si(2)−O(3)−Al	138.1(2)	137.3(2)	136.6(2)	136.5(1)	136.6(7)	136.3(3)	135.6(3)
Si(2)−O(4)−Al	139.0(2)	138.5(1)	137.0(2)	137.1(1)	138.2(7)	136.1(3)	133.9(3)
Si(1)−O(5)−Si(2)	146.3(1)	145.2(1)	143.6(1)	143.61(8)	143.7(5)	142.5(2)	140.3(2)
Na−O(2)	2.40(1)	2.31(2)	2.47(2)	2.57(2)	2.77(2)	2.36(2)	2.31(1)
	2.62(1)	2.68(2)	2.68(2)	2.56(2)	2.27(2)	2.47(2)	2.45(1)
Na−O(3)	2.35(1)	2.37(2)	2.60(2)	2.53(2)	2.31(2)	2.64(2)	2.64(1)
Na−O(4)	2.38(1)	2.33(2)	2.66(2)	2.73(2)	2.83(2)	2.77(1)	2.72(1)
OW1−O(1)	2.88(2)	2.88(3)	2.87(5)	2.81(4)	2.80(4)	2.83(3)	2.88(3)
OW1−O(2)	3.25(2)	3.08(5)	3.22(7)	3.28(5)	3.24(6)	3.22(4)	3.18(4)
OW1−O(5)	2.98(2)	2.98(4)	3.11(5)	3.15(4)	2.95(5)	2.98(4)	2.97(3)
OW1−Na	2.42(2)	2.29(4)	2.47(4)	2.57(4)	2.80(5)	2.45(3)	2.36(3)
	2.42(3)	2.55(4)	2.40(4)	2.31(4)	2.33(4)	2.37(3)	2.37(3)
OW1−OW2			3.09(4)	2.97(4)	2.88(3)	3.00(2)	2.92(2)
			2.80(4)	2.91(4)	3.05(4)	2.89(3)	2.94(2)
OW2−O(1)			2.99(3)	2.97(3)	2.93(3)	2.99(2)	2.86(2)
OW2−O(2)			3.02(3)	3.00(3)	2.65(3)	2.96(2)	2.91(2)
			3.10(3)	3.10(3)	3.18(4)	2.96(2)	2.83(2)
OW2−O(3)			2.83(4)	2.90(3)	3.15(4)	2.74(2)	2.85(2)
OW2−O(4)			2.83(4)	2.78(3)	2.58(4)	2.79(2)	2.50(2)
OW2−O(5)			3.08(3)	2.97(3)	3.09(4)	2.96(2)	3.05(2)
OW2−Na			2.53(3)	2.51(3)	2.47(3)	2.39(2)	2.58(2)

[a] Esd's are in parentheses.

logue of natrolite (ICP, EPMA: $K_{16}Ga_{16}Si_{24}O_{80}\cdot 12H_2O$; the synthesis and the structure of this compound are reported in ref 13) were, in turn, loaded into the DAC at ambient pressure and room temperature along with a few small ruby chips. The DAC is based on a modified Merrill−Bassett design[19] and employs two diamonds with 0.5 mm diameter culets on tungsten−carbide supports. The X-rays are admitted by a 0.5 mm diameter circular aperture, and the exit beam leaves via a 0.5 × 3.0 mm rectangular tapered slit, oriented perpendicular to the horizontal plane of the diffractometer. The sample chamber is provided by a 200 or 350 μm hole formed in the center of a 300 μm thick stainless steel gasket, pre-indented to 100 μm thickness before drilling. A mixture of 16:3:1 by volume of methanol:ethanol:water was used as a pressure transmission fluid, which is known to remain hydrostatic up to ~10 GPa.[20] The pressure at the sample was measured by detecting the shift in the R1 emission line of the included ruby chips.[21] No evidence of nonhydrostatic conditions or pressure anisotropy was detected during our experiments, and the instrumental errors on the pressure measurements ranged between 0.05 and 0.1 GPa. Typically, the sample was equilibrated for about 15 min at each measured pressure. The DAC was then placed at the second axis of the diffractometer, and the sample position was adjusted by using the pre-centered microscope. After the diffraction data measurement, the sample pressure was raised by 0.5−1.0 GPa increments before subsequent data measurements up to 5 GPa. Several pressure points were chosen for diffraction data measurements during pressure release. For natrolite, mesolite, and the gallosilicate natrolite, there was no evidence of stress-induced peak broadening or pressure-driven amorphization and the recovered sample maintained its original white color and crystallinity. For scolecite, the experiment was repeated 5 times, and in all cases the measured diffraction data showed progressive broadening of the peaks at higher pressures up to 5 GPa.

Unit cell parameters were determined by whole pattern fitting using the LeBail method. The diffraction peaks were modeled by varying only a half-width parameter in the pseudo-Voigt profile function. Bulk moduli were calculated by fitting the Murnaghan Equation of State to the normalized volumes ($V/V_0 = [1 + B'P/B_0]^{-1/B'}$, where $B' = (\partial B/\partial P)_{P=0} = 4$).[22] For the data collected on natrolite, Rietveld structure refinements[23,24] were performed using the GSAS suite of programs.[25] The starting framework model at each pressure point was constructed from Distance Least Squares (DLS) minimization,[26] which also provided restraints during the refinement processes. Difference Fourier maps were generated, and sodium and oxygen atoms were used to model the extraframework species Na^+ and water molecules, respectively. Refinements of the fractional site occupancies indicated that these atoms fully

(19) Merrill, L.; Bassett, W. A. *Rev. Sci. Instrum.* **1974**, *45*, 290−294.
(20) Hazen, R. M.; Finger, L. W. *Comparative Crystal Chemistry*; John Wiley & Sons: New York, 1982.
(21) Bell, P. M.; Mao, H. K. *Absolute pressure measurements and their comparison with the ruby* fluorescence (R1) pressure scale to 1.5 Mbar, In *Carnegie Institute Washington Year Book*; Carnegie Institute: Washington, DC, 1979; Vol. 78, pp 665−669.
(22) Angel, R. J. Equations of State. In *High-Temperature and High-Pressure Crystal Chemistry*; Hazen, R. M., Downs, R. T., Eds.; The Mineralogical Society of America: Washington, DC, 2000; Vol. 41, pp 35−58.
(23) Rietveld, H. M. *J. Appl. Crystallogr.* **1969**, *2*, 65−71.
(24) Young, R. A. *The Rietveld Method*; International Union of Crystallography, Oxford University Press: New York, 1995.
(25) Larson, A. C.; VonDreele, R. B. *GSAS; General Structure Analysis System*, Report LAUR 86-748, Los Alamos National Laboratory, New Mexico, 1986.
(26) Meier, W. H.; Villiger, H. *Z. Kristallogr.* **1969**, *129*, 411−423.

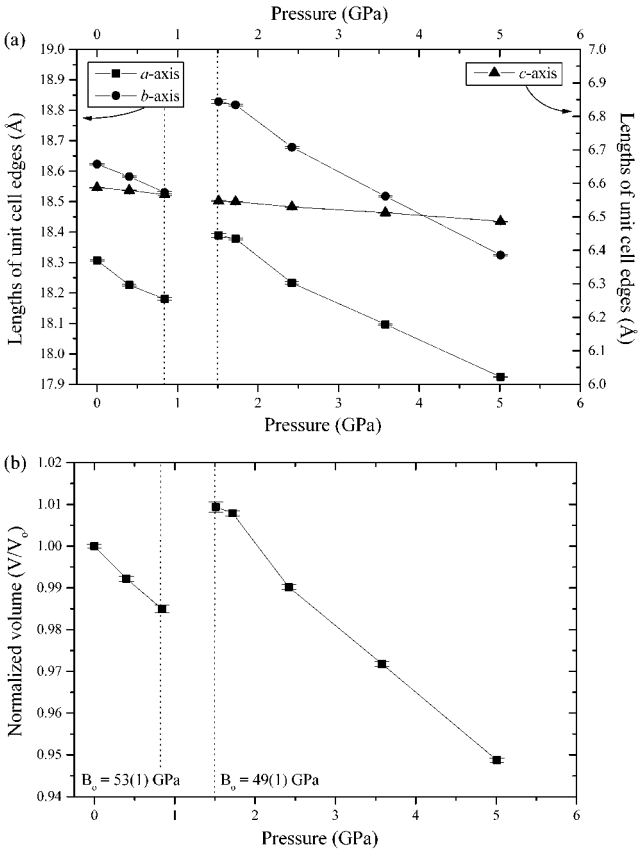

Figure 2. (a) Changes in the unit cell edge lengths (Å) of natrolite as a function of pressure. Estimated standard deviations (esd's) are multiplied by three at each point. The structure model at ambient pressure is from the work of Baur et al.[12] (b) Pressure dependence of the unit cell volume of natrolite, normalized to their ambient pressure value.

occupy the extraframework sites and were subsequently fixed to unity. An overall isotropic displacement parameter was used for the framework atoms; another was used for the nonframework oxygens and cations. Selected refinement results are listed in Tables 1−2.

Results

Natrolite. The evolution of the unit cell parameters of natrolite is shown in Figure 2a. Between 0.8 and 1.5 GPa, the pressure-induced swelling is caused by the expansion of the unit cell along the *a*- and *b*-unit cell axes whereas the *c*-axis shows the expected contraction behavior with pressure throughout the volume expansion period. This 2-dimensional swelling suggests that the rotation of the chains along the *c*-axis and subsequent expansion of the channels in the (001) plane is responsible for the observed volume increase. The calculated bulk modulus of the large-volume natrolite ($B_0 = 49(1)$ GPa) is slightly smaller than that of the normal natrolite ($B_0 = 53(1)$ GPa), illustrating increased compressibility for this high-water-content phase (Figure 2b).

The changes in the crystal structure accompanying the pressure-induced swelling were investigated by performing Rietveld refinements using the framework geometrical restraints and the diffraction data collected in the pressure range examined (see Table 1 for details). The two structural models for the phases before and after the volume expansion are shown in Figure 3 (Table 1). Before the volume expansion, the Na atom maintains its coordination of two water oxygens and four framework oxygens in a distorted trigonal prism. Considering only the extraframework species, the water molecules and the sodium cations bond to form a zigzag chain along the *c*-axis. After the volume expansion at 1.5 GPa, an additional fully occupied water site (OW2) appears along the channel, increasing the crystal water content to 32 H_2O per unit cell (Figure 3, Table 1). This new site has been proposed to be half-filled with water molecules in paranatrolite (24 H_2O per unit cell),[27] which leads to an anomalous increase in the water mobility observed in NMR and other spectroscopic measurements.[8,28] In addition, unlike the sodium−water chains in the low-pressure phase below 0.8 GPa, the superhydration at the OW2 site generates a helical nanotube of hydrogen-bonded water molecules along the *c*-axis (see Discussion and Figure 9).

During the superhydration occurring between 0.8 and 1.5 GPa, peak splittings in the powder diffraction pattern were observed at 1.25 GPa. We initially suspected that at this pressure a pseudoorthorhombic paranatrolite (with disordered water sublattice) or its mixture with the superhydrated orthorhombic natrolite was present. A second set of experiments was performed to investigate more carefully the phases present during superhydration. Several pressure points between 0.8 and 2.0 GPa were chosen to collect diffraction patterns. The measured data were consistent with the existence of two phases during the superhydration and volume expansion. The new phase has a larger unit cell length for the *a*- and *b*-axes (∼18.9 and ∼19.1 Å, respectively) and a smaller *c*-axis (∼6.5 Å) than those of the normal and superhydrated natrolite and shows peak splittings suggesting a pseudoorthorhombic distortion. This is consistent with the presence of paranatrolite with 24 H_2O per unit cell before superhydration increases the water content to 32.[7] More detailed structural investigations of this intermediate high-pressure phase were not possible with the current data. In both runs, diffraction data on the recovered sample underlined the reversibility of the system, with the unit cell parameters being the same as those under ambient conditions (within 3 σ).

The changes in framework geometry were monitored using the T−O−T bond angles within and between the chains (Figure 4). The T−O−T angles within the chain do not follow any systematic changes whereas the bridging T−O2−T angle between the chains shows small changes before and a continuous contraction after the superhydration, respectively. At the same time, the overall chain rotation angle, ψ, increases initially up to 25.7° at 0.8 GPa, then drops to 23.7° during superhydration, and increases back up at 5.0 GPa. This indicates that superhydration is coupled to the relaxation of the overall distortion of the framework by expanding the pore space perpendicular to the channel.

Mesolite. The changes of the unit cell parameters of mesolite are displayed as a function of pressure in Figure 5a, with three representative powder diffraction patterns shown in Figure 6. The high-pressure phase of mesolite above 1.73 GPa is characterized by a 2-dimensionally expanded unit cell along the *a*- and *b*-axes and the absence of superlattice reflections with $k \neq 3n$. The latter is an indication of an order/disorder transition in mesolite and has been observed during its dehydration process where the well-defined natrolite and scolecite layers become indistinguishable upon the loss of the Ca-coordinating water and subsequent disordering of Na and Ca cations throughout

(27) Baur, W. H. *Cryst. Res. Technol.* **1991**, *26*, 169−171.
(28) Gabuda, S. P.; Kozlova, S. G. *J. Struct. Chem.* **1997**, *38*, 562−569.

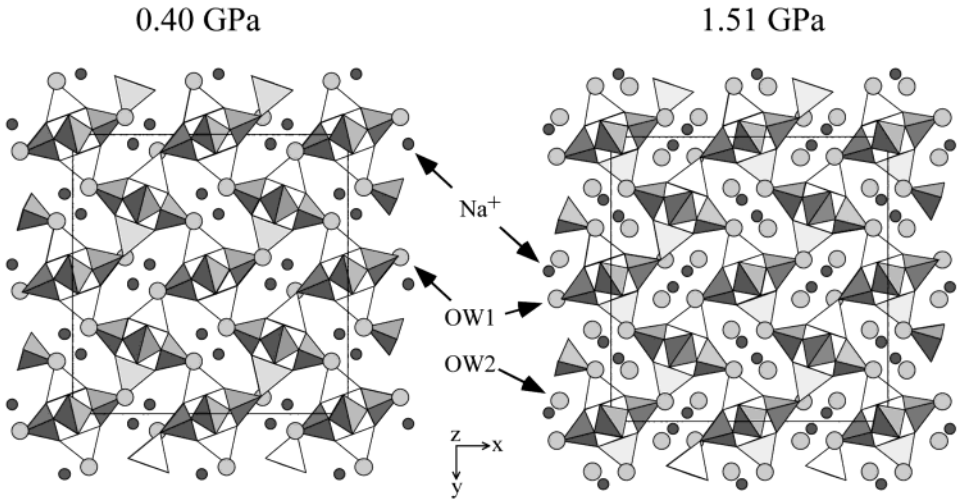

Figure 3. Polyhedral representations of natrolite at 0.40 GPa (left) and at 1.51 GPa (right) viewed along [001], the chain/channel axis. Large-light circles represent water molecules, small-dark ones sodium cations. Dark (light) tetrahedra illustrate an ordered distribution of Si (Al) atoms in the framework. Straight lines define the unit cell.

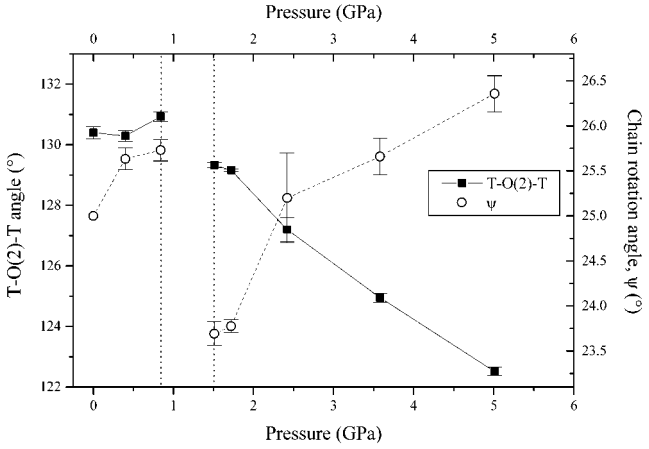

Figure 4. Changes in T−O2−T bond angle and overall chain rotation angle of natrolite as a function of pressure.

the neighboring channels.[29] This is the first observation of a pressure-induced cation disordering in zeolites: it is rather remarkable since in this study a hydration is probably the driving force for the cation disordering rather than the more commonly observed dehydration. Unlike the evolution of the powder diffraction pattern measured in natrolite, there is no manifestation of an intermediate phase between the normal (ordered) and expanded (disordered) phases. Instead, the *a*- and *b*-unit cell lengths increase slightly at 1.19 GPa before the order−disorder transition sets in. In mesolite, the Ca channels already contain 50% more water molecules when compared to the Na channels. As a result, the overall volume increase is only 0.5% compared to 2.5% in natrolite (Figure 5b). When the pressure was released, the mesolite superlattice reflections were recovered with comparable *d* spacings to those before superhydration. The calculated bulk-modulus of the disordered, sublattice phase ($B_0 = 80(10)$ GPa) is smaller than that of the superlattice phase before the volume expansion ($B_0 = 104(1)$ GPa) (Figure 5b). The high-pressure powder diffraction data measured on mesolite sample were not of sufficient quality to locate the new water sites through Rietveld structure refinements.

Scolecite. The high-pressure behavior up to 5 GPa of scolecite, the Ca-endmember of natrolite, does not resemble that of natrolite and mesolite under the same hydrostatic conditions. Powder diffraction data of scolecite from five separate high-pressure runs all show progressive peak broadening along with decreased peak intensities. This effect becomes notable above 2 GPa where, in some cases, a volume expansion is observed by diffraction peaks shifted to lower 2θ values (Figure 7). Pressure-induced amorphization has often been noticed while exploring the high-pressure crystal chemistry of zeolites where quasihydrostatic solid pressure media such as pyrophyllite or KBr are used which are known to exert shear stress on the sample.[30−32] The loss of long-range order in zeolites under moderate hydrostatic pressures, especially here when pore-penetrating liquids are used as a pressure-transmission medium, is therefore an uncommon example of a hydrostatic pressure-induced amorphization effect. When the pressure was released, the crystallinity of the scolecite phase was regained and the overall intensities of the peaks after decompression were close to those before compression. The peaks from the fully released sample have similar *d* spacings as those from the starting material ($d_{(021)} = 6.61(1)$ Å after decompression, $d_{(021)} = 6.62(1)$ Å before compression[33]). We note that the peak measured at $d = 6.55(3)$ Å (just after the (021) in the fully released sample) was not observed in the other runs. It may arise from a mixture of two phases after decompression or indicate a splitting of (021) at the higher pressures to which this sample was subjected. Further analysis of the data was not possible due to the poor peak resolution and peak-to-background ratio for this pseudoorthorhombic analogue.

Potassium Gallosilicate Analogue of Natrolite. The changes of the unit cell parameters of the potassium gallosilicate natrolite as a function of pressure are shown in Figure 8a. The volume

(29) Stahl, K.; Hanson, J. *J. Appl. Crystallogr.* **1994**, *27*, 543−550.

(30) Greaves, G. N. Zeolite instability and collapse. In *Phase Transitions and Self-Organization in Electronic and Molecular Networks*; Phillips, J. C., Thorpe, M. F., Eds.; Kluwer Academic: Dordrecht, The Netherlands, 2001; pp 225−246.
(31) Gillet, P.; Malezieux, J.-M.; Itie, J.-P. *Am. Mineral.* **1996**, *81*, 651−657.
(32) Rutter, M. D.; Uchida, T.; Secco, R. A.; Huang, Y.; Wang, Y. *J. Phys. Chem. Solids* **2001**, *62*, 599−606.
(33) Smith, J. V.; Pluth, J. J.; Artioli, G.; Ross, F. K. In *Proceedings of the 6th International Zeolite Conference*; Olson, D. H., Bisio, A., Eds.; Butterworth: Guildford: Reno, 1983; pp 842−850.

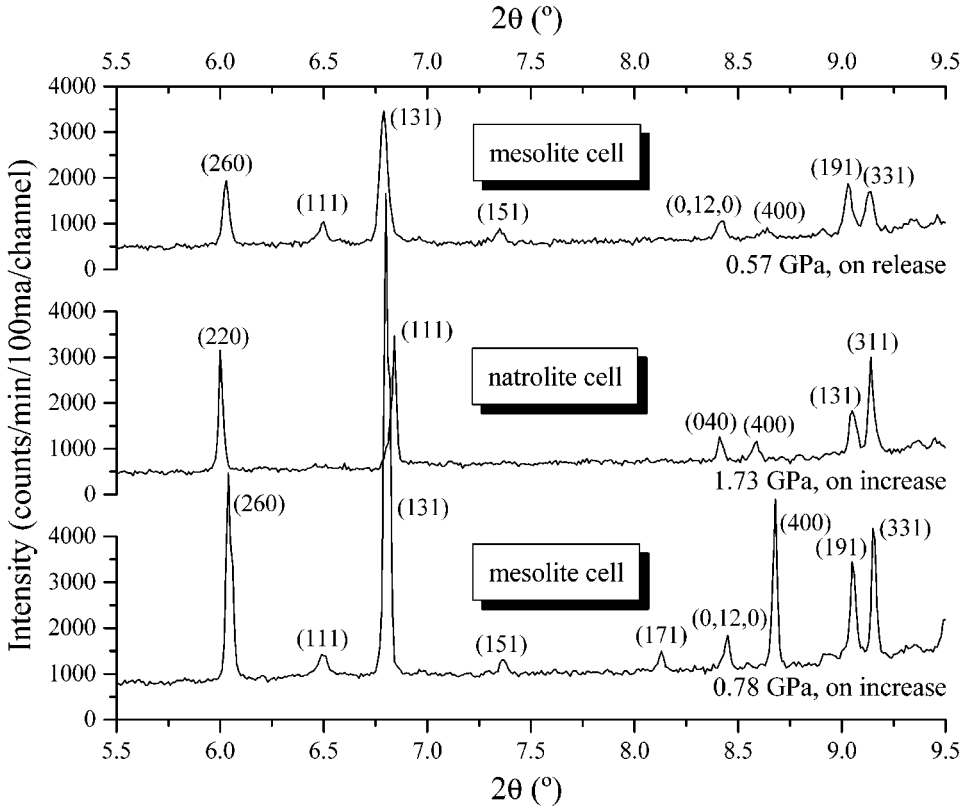

Figure 5. Details of the powder diffraction patterns of mesolite as a function of pressure. Note the disappearance of the $k \neq 3n$ reflections at 1.73 GPa, which revert back on pressure release.

expansion of about 1.0% occurs between 1.24 and 1.71 GPa (Figure 8b). The manner in which this expansion takes place in this material is, however, different from that observed in natrolite and mesolite: it shows a 3-dimensional swelling. The *c*-axis, along which the rigid T_5O_{10} tetrahedral building units join to form the fibrous chain, expands by ca. 0.4% in the gallosilicate natrolite whereas it contracts in natrolite and mesolite upon compression. More strikingly, when releasing pressure the larger volume phase, probably superhydrated, is stabilized. The unit cell volume of the recovered sample is 0.7% larger than the one measured before compression. To follow the changes in the unit cell volume as a function of time, sets of diffraction data were collected 3 and 8 days after pressure release. There was no indication of a further volume contraction and the cell constants were the same as those measured right after ending the pressure cycle (within 2σ). The overall intensity of the peaks decreases slightly as pressure increases. The shape of the peaks, however, does not show any degradation, suggesting pressure-induced amorphization does not occur in this material under hydrostatic conditions up to 4 GPa. Compressibility of the expanded phase above 1.71 GPa ($B_0 = 59(5)$ GPa) is slightly larger than that of the phase before the volume expansion ($B_0 = 66(7)$ GPa), consistent with the trend found in natrolite and mesolite (Figure 8b). Further structure refinements using these data were not successful due to the significant overlap of the reflections with the backgrounds from the gasket material above 18° in 2θ.

Discussion

Superhydration and Volume Expansion Under Pressure. The arrangement of nonframework cations and water molecules inside the natrolite channels before and after superhydration is depicted in Figure 9. The 2-dimensional swelling between 0.84 and 1.51 GPa corresponds to a decrease in the ellipticity of the helical 8-ring channel by 6.7% (the ellipticity is defined by the ratio between the shortest to longest framework oxygen distances of the channel opening: the shortest O2−O2 distance across the channel increases from 4.70(1) to 4.94(1) Å upon superhydration). This is compatible with the changes in the Na coordination environment. At 0.84 GPa just before superhydration, the sodium cation is coordinated by four framework oxygens and two water molecules with a strong Na−O2 bond with an interatomic distance of 2.31(2) Å (Table 2). After superhydration at 1.51 GPa, the sodium coordination changes to 7-fold by binding an additional water molecule, which weakens the bonding between the sodium and the framework oxygens; the shortest bonding distance to the framework oxygen (Na−O2) is now 2.47(2) Å with the distance to the new water oxygen (Na−OW2) being 2.53(3) Å (Table 2). As a result, the sodium cations in the superhydrated natrolite have stronger interactions with water molecules than the framework oxygens; the sodium to framework oxygen distances range from 2.47(2) to 2.68(2) Å whereas the interatomic distances to water oxygens are within 2.40(4) and 2.53(3) Å (Table 2). This is analogous to the Ca-bonding in mesolite and scolecite where the Ca cations are strongly coordinated by three water molecules (2.31−2.36 Å) and to a lesser extent to four framework oxygens (2.50−2.54 Å).[15] We predict that superhydration and the associated increase of the pore openings, as well as the decrease in the Na to framework oxygen interaction, will cause modifications to the ion exchange properties in this class of small-pore zeolites.

It is also interesting to comment on the structure of the water

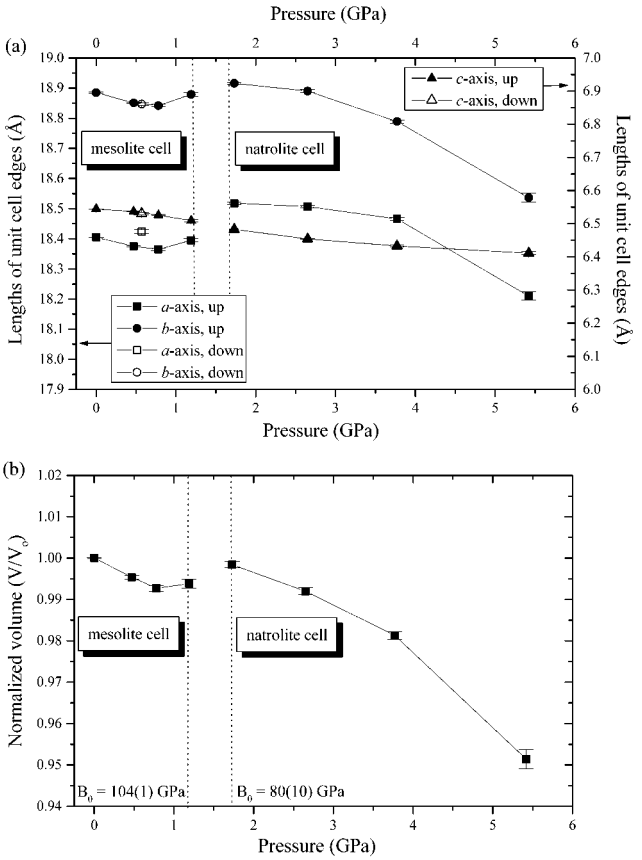

Figure 6. (a) Changes in the unit cell edge lengths (Å) of mesolite as a function of pressure. The *b*-axis lengths in the mesolite region represent $b_{mesolite}/3$. Esd's are multiplied by three at each point. The values at ambient pressure are derived from the work of Artioli et al.[15] (b) Pressure dependence of the unit cell volume of mesolite, normalized to their ambient pressure value.

molecules inside the aluminosilicate channels after superhydration (Figure 9). Before superhydration, there are no hydrogen bonds between water molecules, whereas upon superhydration every water molecule is hydrogen bonded to exactly three nearest-neighboring waters. The first two hydrogen bonds form inside the channel with O−O interatomic distances of 2.80(4) and 3.09(4) Å and O−O−O angles of 104(2) and 112(1)° (according to the 1.51 GPa model, Table 2). This results in the formation of a helical water nanotube along the natrolite channel with sodium cations inside. The other hydrogen bond is relatively weak (3.14(3) Å, 1.51 GPa model) and interconnects neighboring water nanotubes across the channel wall via the $T_{10}O_{20}$ window. The helical water nanotube can be described as having a negatively charged exterior near the aluminosilicate framework and positively charged sodium cations inside. This suggests that these water molecules are highly oriented within and between the nanotubes. As mentioned previously, this helical water nanotube is responsible for the anomalous increase in the water diffusion at high pressure.[7,8] It has also been shown that changes in local channel polarity and solvent conditions can be used to modify the water occupancy and its conductivity inside a carbon nanotube.[34] We suspect that the water diffusivity of the superhydrated natrolite can be tuned by changes in the composition of the nonframework cations or the framework Al/Si ratio (and possibly framework composition). Furthermore, increase in the channel diameter or the compression of the increased number of water molecules may induce formation of different water structures as demonstrated in the example of ordered ice nanotubes inside various sizes of carbon nanotubes.[35] The conditions used for superhydration in this work resemble part of the cold oceanic lithosphere during subduction,[36,37] which implies zeolite superhydration should be considered as a possible mechanism for the storage and transport of water into the Earth's upper mantle. Our investigation will expand to other dense hydrous phases of geochemical importance such as phillipsite or lawsonite, and also to higher pressures.

Pressure-Induced Cation Disordering. Temperature-induced cation disordering occurs in mesolite as a result of changes in Ca coordination.[29] Upon heating, one of the Ca-coordinating waters, unique in the Ca layer, starts to be expelled preferentially. Complete exclusion of the water results in the reduction of the Ca-coordination number from seven to six, which is the same as the Na-coordination number in the Na layer. As a consequence, Ca and Na atoms can then randomly occupy the former Na sites in the natrolite cell, with the water molecules fully occupying the natrolite water site. At this stage, there is no distinction between the natrolite and scolecite layers along the *b*-axis, and this is indicated by the disappearance of the mesolite superlattice reflections.[29]

Assuming that the volume expansion in mesolite indicates superhydration, the mechanism of the pressure-induced cation disordering must be different from its temperature-driven analogue. Superhydration in mesolite is likely to occur preferentially in the Na layer rather than in the Ca layer since the latter already contains 50% more water at ambient conditions. This will cause an increase in the Na-coordination number from six to seven, as in natrolite, which will make the Na coordination shell compatible to the Ca shell. This will facilitate cross-channel diffusion and subsequent disordering of both cations. The slight increase in the volume before the disappearance of the superlattice reflections implies that the cation disordering is a continuous transition driven by diffusion processes, and the reappearance of the superlattice reflections upon pressure release indicates reversible hydration/dehydration. At this time we cannot rule out other mechanisms of cation disordering, such as superhydration in the Ca layer leading to disordering of the Ca atoms in such a way as to destroy the scattering contrast between layers. High-pressure single-crystal diffraction studies are planned to provide the structural details on the disordering phenomenon in mesolite.

Hydrostatic Pressure-Induced Partial Amorphization. Using KBr as a solid pressure transmission media, Gillet et al. reported pressure-induced amorphizations in scolecite and mesolite.[31] In the absence of the pore-penetrating molecules such as water, both samples showed progressive reduction in intensity and broadening of the X-ray and Raman peaks without any indications of phase transitions and completely amorphized above 10 GPa. These transitions were described as irreversible and the pressure-quenched products were similar to the temperature-quenched aluminosilicate glasses. The results of our five separate high-pressure runs of scolecite are also indicative, although not conclusive, of the effects of a hydrostatic pressure-

(34) Hummer, G.; Rasaiah, J. C.; Noworyta, J. P. *Nature* **2001**, *414*, 188−190.
(35) Koga, K.; Gao, G. T.; Tanaka, H.; Zeng, X. C. *Nature* **2001**, *412*, 802−805.
(36) Thompson, A. B. *Nature* **1992**, *358*, 295−302.
(37) Bina, C. R.; Navrotsky, A. *Nature* **2000**, *408*, 844−847.

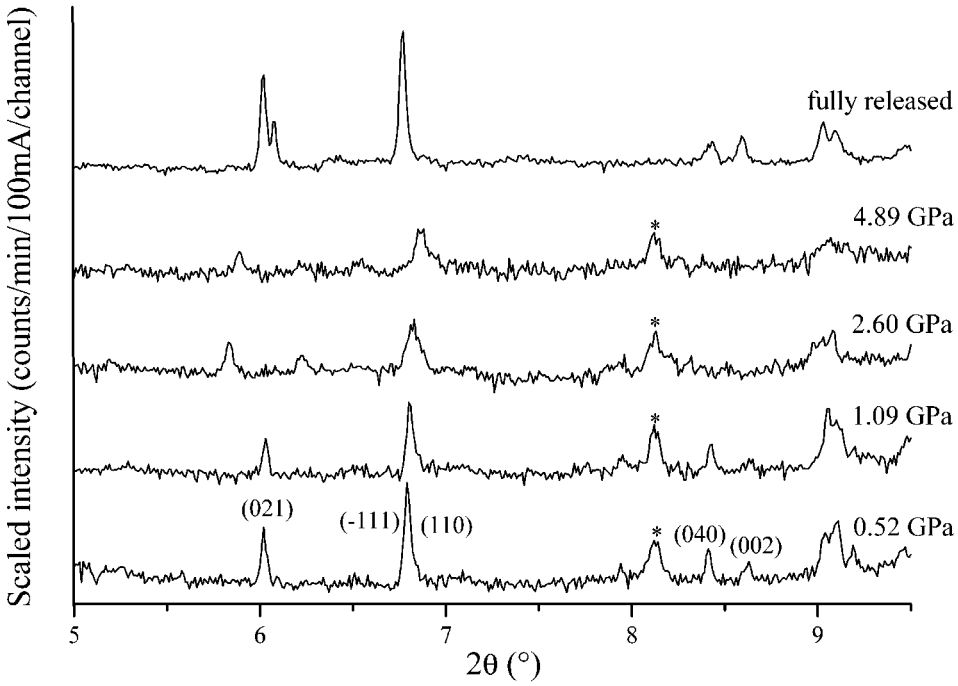

Figure 7. Details of the powder diffraction patterns of scolecite as a function of pressure. The other four high-pressure runs showed similar broadening and reduction in intensity of the diffraction peaks above 2 GPa. An asterisk identifies the $\lambda/2$ component from the gasket metal.

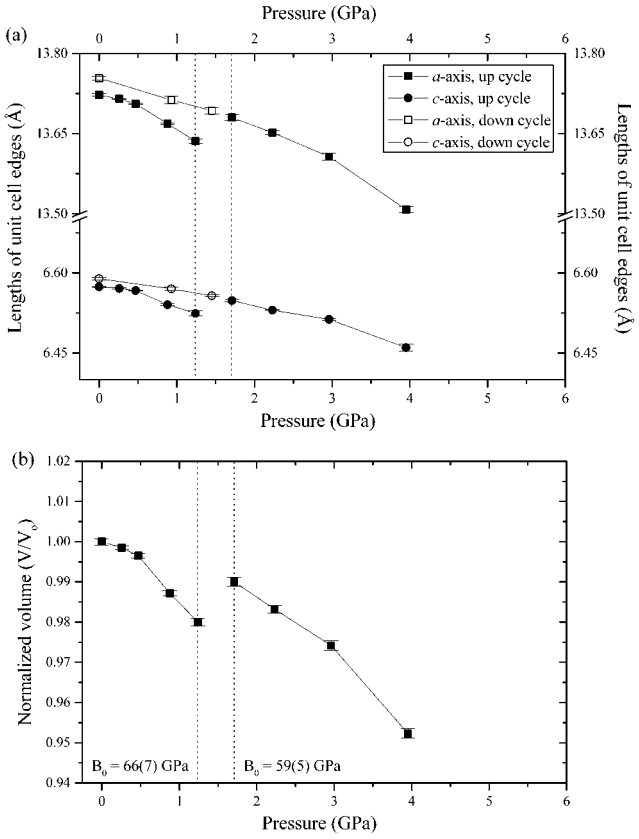

Figure 8. (a) Changes in the unit cell edge lengths (Å) of the gallosilicate natrolite as a function of pressure. Esd's are multiplied by three at each point. The starting values at ambient pressure are calculated from powder diffraction data measured using a flat plate sample. (b) Pressure dependence of the unit cell volume of the gallosilicate natrolite, normalized to their ambient pressure value.

induced amorphization. There is a 40% reduction of $I_{(021)}$ and a 30% increase in the $fwhm_{(021)}$ between 0.52 and 2.60 GPa, while the width of the R1 ruby emission line did not show any broadening. Important differences between our results and those of Gillet et al. lie in the choice of the pressure medium; the solid pressure medium produces quasihydrostatic pressures and shear stress on the sample whereas the alcohol and water mixture in the optimum ratio provide much better hydrostatic conditions.[20] Furthermore, as this study clearly shows, the ability of the water molecules to penetrate the nanopore space and interact with the species inside provides an additional variable in the high-pressure phase transitions. Unlike the results from Gillet et al., we observed some indications of volume expansion in scolecite above 2 GPa (3% increase on $d_{(021)}$ between 0.52 and 2.60 GPa data), which is in line with the superhydration or volume expansion behaviors found in natrolite and mesolite. Furthermore, the reappearance of the peaks at similar *d* spacings upon decompression indicates that the local structures are maintained throughout the X-ray amorphous region, which may suggest that shear stress is not the major cause for the amorphization. A similar phenomenon has been shown to occur in zeolite LTA,[32] and these materials are said to have a structural memory or templating nondeformable units about which the original crystal structure can be restructured upon pressure release.[38] The mechanism of the pressure-induced amorphization in this Ca-endmember of the natrolite family needs further investigation. The use of pair-distribution function will be potentially important in probing the local structural changes in the pressure-amorphous region.

3-Dimensional Swelling and Irreversible Volume Expansion. The different type of pressure-induced expansion observed in the potassium gallosilicate natrolite can be related to the different cation and water distribution in the starting materials. Unlike natrolite, mesolite, and scolecite, the potassium cations in the gallosilicate natrolite occupy the sites close to the channel

(38) Tse, J. S.; Klug, D. D.; Ripmeester, J. A.; Desgreniers, S.; Lagarec, K. *Nature* **1994**, *369*, 724−727.

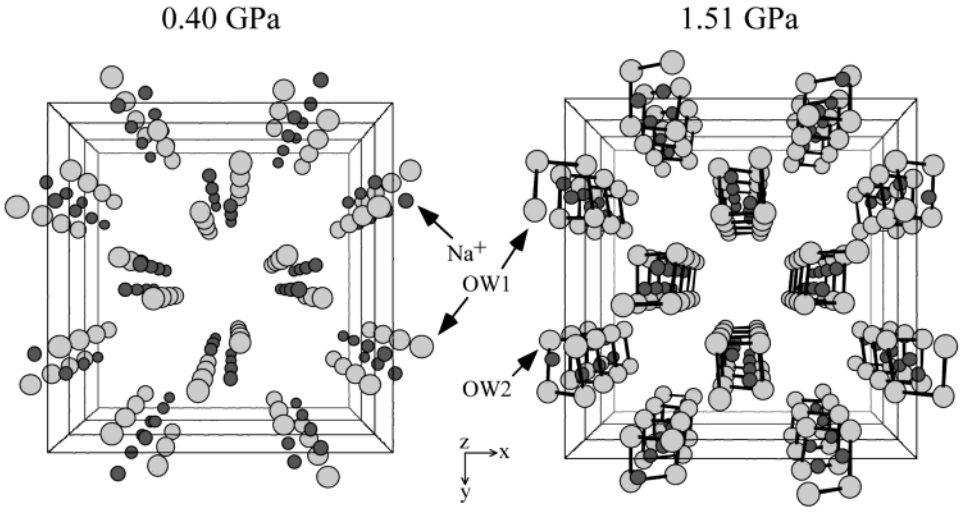

Figure 9. The structure of the nonframework species found in natrolite at 0.40 GPa (left) and at 1.51 GPa (right) viewed perspectively along the *c*-axis. Note the formation of the hydrogen-bonded water nanotube at 1.51 GPa. Large-light circles represent water molecules, small-dark ones sodium cations. Straight lines define unit cells, short bars hydrogen bonds.

walls bound by the $T_{10}O_{20}$ windows, and the sites along the channels host disordered water molecules at ambient conditions.[13] The cation distribution in the gallosilicate natrolite likely remains more or less the same throughout the volume expansion at high pressures since there are no major changes in the relative peak intensities. If additional water molecules are added at high pressure to drive the observed 3-dimensional volume expansion, the resulting pore water must have a different structure to the one observed in superhydrated natrolite. In addition to the different distribution of the nonframework species, another reason for the 3-dimensional swelling in the gallosilicate natrolite may be attributed to the flexibility of the T−O−T angles in a Ga/Si framework compared to its Al/Si counterpart. Due to the substitution of the larger Ga for Al, the T−O−T angles in the gallosilicate frameworks show greater degrees of distortions than those of the aluminosilicates.[13,39] Given the higher flexibility of the T−O−T angle in a gallosilicate framework, incorporation of additional water molecules into the channels at high pressure would exert the T−O−T angles within the fibrous chain to relax along with the angles between the chains. Due to these characteristics, the expanded gallosilicate phase at high pressures is found to be metastable under ambient conditions. The preservation of the expanded phase after decompression, which is presumably superhydrated, implies the potential use of similar systems with a superhydration at lower pressures as, for example, a storage media for the tritiated water (THO) from nuclear processing facilities. Structural details of volume expansion in this analogue of the natrolite family are being investigated further using high-pressure recovered single crystals.

(39) Tripathi, A.; Parise, J. B.; Kim, S. J.; Lee, Y. J.; Uh, Y. S. *Acta Crystallogr.* **2001**, *C57*, 344−346.

Conclusion

All the zeolites with the natrolite framework topology investigated here showed volume expansion at moderately high pressures, i.e., below 2 GPa. On the basis of the result from the natrolite study, the high-pressure swellings in this family of small-pore zeolites are expected to be driven by the incorporation of additional water molecules into the respective nanochannels from the pressure-transmission fluid. The type of pressure-induced volume expansion, and accompanying superhydration, depends both on the nonframework charge-balancing cations and the framework compositions, implying the superhydration can be further tailored and applied for specific applications. Modifications of the nanopore geometry and cation coordination observed upon superhydration point toward novel properties of zeolites under pressure. We intend to establish the ion exchange properties in this family of zeolites under high pressure.

Acknowledgment. This work was supported by an LDRD from BNL (Pressure in Nanopores). J. Parise appreciates grants from the ACS-PRF and NSF-DMR-0095633. S.-J. Kim of KIST is acknowledged for the synthesis of the potassium gallosilicate natrolite. The authors thank Jeffrey Post of the National Museum of Natural History at the Smithsonian Institution for providing the mineral specimens and Aaron Celestian and Prof. Donald Lindsley of Stony Brook University for chemical analyses. Research carried out in part at the NSLS at BNL is supported by the U.S. DoE (DE-Ac02-98CH10886 for beamline X7A). We gratefully acknowledge the Geophysical Laboratory of the Carnegie Institute for access to their ruby laser system at beamline X17C.

JA0255960